CrossMark

ORIGINAL ARTICLE

Tidal effects in differentiated viscoelastic bodies: a numerical approach

M. Walterová[1] · **M. Běhounková**[1]

Abstract The majority of confirmed terrestrial exoplanets orbits close to their host stars and their evolution was likely altered by tidal interaction. Nevertheless, due to their viscoelastic properties on the tidal frequencies, their response cannot be described exactly by standardly employed constant-lag models. We therefore introduce a tidal model based on the numerical evaluation of a continuum mechanics problem describing the deformation of viscoelastic (Maxwell or Andrade) planetary mantles subjected to external force. We apply the method on a model Earth-size planet orbiting a low-mass star and study the effect of the orbital eccentricity, the mantle viscosity and the chosen rheology on the tidal dissipation, the complex Love numbers and the tidal torque. The number of stable spin states (i.e., zero tidal torque) grows with increasing mantle viscosity, similarly to the analytical model of Correia et al. (Astron Astrophys 571:A50, 2014) for homogeneous bodies. This behavior is only slightly influenced by the rheology used. Similarly, the Love numbers do not distinctly depend on the considered rheological model. The increase in viscosity affects the amplitude of their variations. The tidal heating described by the Maxwell rheology attains local minima associated with low spin-orbit resonances, with depth and shape depending on both the eccentricity and the viscosity. For the Andrade rheology, the minima at low resonances are very shallow and the tidal heating for all viscosities resembles a "fluid limit." The tidal heating is the quantity influenced the most by the rheology, having thus possible impact on the internal thermal evolution.

✉ M. Walterová
kanova@karel.troja.mff.cuni.cz

M. Běhounková
behounek@karel.troja.mff.cuni.cz

1   Department of Geophysics, Faculty of Mathematics and Physics, Charles University, Prague, Czech Republic

1 Introduction

Following the first detection of a planet orbiting a main-sequence star other than the Sun (Mayor and Queloz 1995), the past two decades have witnessed the birth and successive rapid development of exoplanetary science. The number of confirmed exoplanets increases each year and, due to improvements in both the observation and the data reduction, even small bodies of masses comparable to the Earth become detectable and characterizable (e.g., Weiss and Marcy 2014; Mullally et al. 2015; Zeng et al. 2016 and many others). Among the rocky worlds discovered by indirect techniques, the majority orbits very close to their host star and is presumably subjected to intensive tidal loading, resulting eventually into enhanced heating of the planetary interior, secular despinning and circularization of the orbit.

The first comprehensive mathematical theory of Earth tides was formulated by George Darwin in his works from the 1870s and 1880s (e.g., Darwin 1880) and generalized by William Kaula in the 1960s (Kaula 1961, 1964). Throughout the second half of the twentieth century, many other authors greatly contributed to the theory, explaining a variety of phenomena related to the tidal interaction and exploring new ways of their description (e.g., Gerstenkorn 1955; MacDonald 1964; Goldreich 1966; Goldreich and Soter 1966; Singer 1968; Mignard 1979; Néron de Surgy and Laskar 1997). Darwin's and Kaula's method, consisting in Fourier expansion of the tidal and the disturbing potential, enables estimation of tidal effects in homogeneous bodies governed by any rheology, under the condition that each mode of the expansion can be treated as independent on the other modes. A rheological model of the body is inserted into the tidal equations through the potential Love number k and the phase lag ε, which is related to the quality factor Q of the planet by $Q^{-1} = \sin |\varepsilon|$.

Both parameters can be, in general, frequency dependent and a consistent theory derives their functional form from basic rheological considerations (e.g., Castillo-Rogez et al. 2011). However, owing to the lack of data, the Love number of exoplanets has often been treated as constant and equal to the values measured for the Earth or the other planets and moons of the Solar system. Similarly, the phase lag between the tidal and the disturbing potential is assumed to be constant in a number of studies (e.g., Kaula 1964; Goldreich 1966; Barnes et al. 2009). Such an assumption, corresponding to the assumption of constant tidal Q, is underlied by measurements of seismic wave attenuation in a wide range of frequencies (Goldreich and Soter 1966; Kjartansson 1979). Its implications for the tidal torque acting on the entire planetary body during its revolution around the host star are, however, not fully justified (see e.g., Makarov and Efroimsky 2013).

Another class of models prescribes a linear dependence of the phase lag on the loading frequency, or a constant time lag (e.g., Singer 1968; Mignard 1979; Néron de Surgy and Laskar 1997; Correia and Laskar 2010). The constant time lag model was originally derived by Darwin (1880) for bodies exhibiting low viscosity and negligible rigidity. Its applicability is therefore limited to a specific range of bodies, preferentially to gaseous planets and stars (for a more precise discussion of the limitations, see Makarov and Efroimsky 2013). In the context of the tidal evolution of binary stars, this model is known as the "weak friction" approximation (e.g., Alexander 1973; Hut 1981).

Although the simplified constant-lag models are applicable in particular cases, the response of terrestrial planets and moons subjected to tides is more adequately characterized by viscoelastic rheologies, where neither the phase lag, nor the time lag is a constant value. Efroimsky and Lainey (2007) introduced a tidal model based on thorough geophysical considerations, with the phase lag proportional to a negative power of the tidal frequency. A special case of this functional dependence is obtained if we describe the planetary body

by the Andrade rheology. da Andrade (1910) measured the stretching of metal wires under constant stresses and found, that in addition to the elastic and the viscous effects, there is a transient component of the deformation, gradually dying out in time. Similar results were later obtained for silicate rocks and ices (Tan et al. 1997; McCarthy et al. 2007). In addition to the laboratory measurements, there is a seismological and geodetical evidence for applicability of the Andrade model on the solid Earth (for a summary see Efroimsky 2012). The transient component, describing the anelastic behavior of the material, becomes important in the case of high-frequency loading, while in the low-frequency domain the reaction is well described by more simple Maxwell rheology.

Due to their better agreement with observation and despite their complexity, viscoelastic models are slowly finding their way to the studies of tidal evolution. Segatz et al. (1988) use the Maxwell model for the calculation of tidal dissipation in Io and Henning et al. (2009) analyze tidal heating in a hot exo-Earth for three viscoelastic rheologies. Combination of the Maxwell and the Andrade model was employed also for considerations of internal and rotational dynamics (e.g., Castillo-Rogez et al. 2011; Makarov and Efroimsky 2013). An internally consistent analytical model of the tidal deformation and long-term orbital evolution of planets described by the Maxwell rheology was approached in two distinct ways by Ferraz-Mello (2013) and Correia et al. (2014). The latter study was extended by Boué et al. (2016) to apply also to planets with nonzero obliquity.

The importance of analytical models lies in their ability to effectively parametrize and explore the main features of tidal evolution. Appropriate parametrization enables utilization of effective and precise time schemes for the computation of long-term processes, including the secular variations of orbital parameters. Most analytical models of tides are, however, describing the planet as a homogeneous sphere. If we are interested in the effects of the internal structure on the tidal deformation and internal heating, it is necessary to proceed to numerical simulations. As a recent example, Frouard et al. (2016) presented a general numerical model of tides on viscoelastic bodies described by the Kelvin–Voigt rheology. Their approach is based on an N-body simulation of gravitating particles connected together in a spring-dashpod network, and therefore represents an alternative to our method.

In this paper, we introduce a numerical model enabling the computation of the tidal torque and the tidal heating inside of a possibly nonhomogeneous mantle of rocky exoplanets. The model of a viscoelastic mantle governed by either the Maxwell or the Andrade rheology is described in Sect. 2, with further details on the numerical scheme provided in "Appendix A." Section 3 is dedicated to the parameter dependence of tidal torque, with qualitative comparison of our results for the Maxwell model with the work of Correia et al. (2014). In Sect. 4, we present a parameter study of tidal heating, showing substantial difference between the predictions of both rheological models. Finally, the two traditional tidal parameters—the Love number k and the phase lag ε—are discussed in Sect. 5.

2 Model

The model planet is a spherical body composed of a solid inner core, liquid outer core and a viscoelastic mantle, described either by the Maxwell or the Andrade rheology. We compute the deformation and stress field solely inside of the mantle, which is assumed to be incompressible and hydrostatically prestressed, and neglect the deformations and dissipation in the core, as well as the core-mantle friction. For the sake of simplicity, we also neglect the tides raised by the planet on the host star.

If the deformations are small compared to the overall size of the body, we may use the linear approximation and write the Eulerian governing equations, representing the mass conservation and the linear momentum conservation (neglecting inertia), as (Tobie et al. 2008; Běhounková et al. 2015; Souček et al. 2016)

$$\nabla \cdot \mathbf{u} = 0, \tag{1}$$

$$-\nabla \pi + \nabla \cdot \mathbf{D} = -\rho_{\mathrm{M}} \mathbf{f}, \tag{2}$$

with a constitutive equation

$$2\varepsilon = \frac{1}{\mu} \mathbf{D} + \int_0^t \frac{1}{\eta} \mathbf{D}(t') \, \mathrm{d}t' + \int_0^t \mu^{\alpha-1} \left(\frac{t-t'}{\zeta \eta} \right)^\alpha \dot{\mathbf{D}}(t') \, \mathrm{d}t' \tag{3}$$

and linearized boundary conditions expressing the force equilibrium on the undeformed boundaries (e.g., Souček et al. 2016)

$$(-\pi \mathbf{I} + \mathbf{D}) \cdot \mathbf{e}_{\mathrm{r}} + u_{\mathrm{r}} \, \rho_{\mathrm{M}} \, g_{\mathrm{s}} \, \mathbf{e}_{\mathrm{r}} = \mathbf{0} \quad \text{on the upper boundary} \tag{4}$$

and

$$(-\pi \mathbf{I} + \mathbf{D}) \cdot \mathbf{e}_{\mathrm{r}} - u_{\mathrm{r}} \, (\rho_{\mathrm{C}} - \rho_{\mathrm{M}}) \, g_{\mathrm{b}} \, \mathbf{e}_{\mathrm{r}} = -\rho_{\mathrm{C}} \, \mathcal{U} \, \mathbf{e}_{\mathrm{r}} \quad \text{on the lower boundary.} \tag{5}$$

Here, $\mathbf{u}$ is the displacement vector, $\varepsilon = \frac{1}{2}(\nabla \mathbf{u} + \nabla^T \mathbf{u})$ stands for the incremental strain tensor, π and $\mathbf{D}$ are the isotropic and the deviatoric parts of the incremental Cauchy stress tensor, $\mathbf{f} = \nabla \mathcal{U}$ represents the body force per unit mass, η and μ are the viscosity and the rigidity (shear modulus) of the mantle, respectively, and α and ζ are empirically given parameters of the Andrade rheology. For the boundary conditions, ρ_{C} is the density of the liquid outer core, ρ_{M} denotes the density of the mantle, g_{s} and g_{b} are the mean gravity accelerations on the upper and the lower boundary, $\mathbf{I}$ is the identity matrix, $\mathbf{e}_{\mathrm{r}}$ is the radial unit vector and $u_{\mathrm{r}} = \mathbf{u} \cdot \mathbf{e}_{\mathrm{r}}$ represents the radial component of the displacement.

Equation (3) in general holds for the Andrade rheology: its first term represents the instantaneous elastic reaction, while the other two terms account for the viscous and the anelastic creep, respectively. A constitutive equation for the linear Maxwell rheology can be obtained by excluding the last term, that is

$$2\varepsilon = \frac{1}{\mu} \mathbf{D} + \int_0^t \frac{1}{\eta} \mathbf{D}(t') \, \mathrm{d}t'. \tag{6}$$

The body force $\mathbf{f}$ (and accordingly the potential $\mathcal{U}$) in our model consists of three parts: the tidal force $\mathbf{f}_{\mathrm{t}}$ due to the host star, the centrifugal force $\mathbf{f}_{\mathrm{cf}}$ due to planet rotation and the self-gravity $\mathbf{f}_{\mathrm{self}}$ induced by the tidal deformation. First, we will focus on the tidal force. The model planet with mass m orbits a star with mass M_* and its orbit is described by the semi-major axis a and the eccentricity e. The star is considered spherical and the planet's obliquity is, for the sake of simplicity, assumed to be zero. At each instant of time, the tidal force acting on a unit volume with planetocentric coordinates $\mathbf{r}' = (r', \vartheta', \varphi')$ due to a disturbing body at coordinates $\mathbf{r} = (r, \vartheta_*, \varphi_*)$ can be written as

$$\mathbf{f}_{\mathrm{t}} \left(r', \vartheta', \varphi' \right) = \sum_{lm} f_{lm}^{l-1}(r') \mathbf{Y}_{lm}^{l-1} \left(\vartheta', \varphi' \right), \tag{7}$$

where $\mathbf{Y}_{lm}^{l-1}$ are vector spherical harmonics (see "Appendix B" or, e.g., Varshalovich et al. 1988) and coefficients f_{lm}^{l-1} are given by

$$f_{lm}^{l-1}(r') = \frac{\mathcal{G}M_*}{r^2} \, 4\pi \sqrt{\frac{l}{2l+1}} \left(\frac{r'}{r}\right)^{l-1} \bar{Y}_{lm}(\vartheta_*, \varphi_*), \tag{8}$$

with $\mathcal{G}$ being Newton's gravitational constant and bar above Y_{lm} symbolizing complex conjugation. The instantaneous distance of the planet from the star is $r = a(1 - e \cos E(t))$ and the eccentric anomaly $E(t)$ is obtained from the iteratively solved Kepler equation. Similarly, the tidal potential can be decomposed into spherical harmonics as

$$\mathcal{U}_t\left(r', \vartheta', \varphi'\right) = \sum_{lm} v_{lm}(r') Y_{lm}\left(\vartheta', \varphi'\right) \tag{9}$$

with coefficients

$$v_{lm}(r') = \frac{\mathcal{G}M_*}{r} \frac{4\pi}{2l+1} \left(\frac{r'}{r}\right)^{l} \bar{Y}_{lm}(\vartheta_*, \varphi_*). \tag{10}$$

The centrifugal force and the centrifugal potential depend on the rotational frequency of the planet Ω_{rot} through

$$\mathbf{f}_{cf}(r', \vartheta', \varphi') = \frac{\sqrt{16\pi}}{3} \Omega_{\text{rot}}^2 r' \mathbf{Y}_{00}^1(\vartheta', \varphi') + \frac{\sqrt{8\pi}}{3} \Omega_{\text{rot}}^2 r' \mathbf{Y}_{20}^1(\vartheta', \varphi') \tag{11}$$

and

$$\mathcal{U}_{cf}(r', \vartheta', \varphi') = -\sqrt{\frac{4\pi}{9}} \Omega_{\text{rot}}^2 (r')^2 Y_{00}(\vartheta', \varphi') + \sqrt{\frac{4\pi}{45}} \Omega_{\text{rot}}^2 (r')^2 Y_{20}(\vartheta', \varphi'). \tag{12}$$

Finally, using the Helmert's method of condensation (Helmert 1884), the effect of self-gravity inside of the homogeneous mantle is introduced by

$$\mathbf{f}_{self}\left(r', \vartheta', \varphi'\right) = 4\pi\mathcal{G} \sum_{lm} \left\{ \sqrt{\frac{l+1}{2l+1}} \, (\rho_C - \rho_M) \, \left(u_r^b\right)_{lm} \left(\frac{r_b}{r'}\right)^{l+2} \mathbf{Y}_{lm}^{l+1}\left(\vartheta', \varphi'\right) \right.$$
$$\left. + \sqrt{\frac{l}{2l+1}} \, \rho_M \left(u_r^s\right)_{lm} \left(\frac{r'}{r_s}\right)^{l-1} \mathbf{Y}_{lm}^{l-1}\left(\vartheta', \varphi'\right) \right\}, \tag{13}$$

where indices "b" and "s" denote the lower and the upper boundary, respectively, and $(u_r)_{lm}$ are spherical harmonic coefficients of the radial component of displacement, related to the coefficients of displacement vector u_{lm}^n at any radius r' by

$$(u_r)_{lm} = \sqrt{\frac{l}{2l+1}} \, u_{lm}^{l-1}(r') - \sqrt{\frac{l+1}{2l+1}} \, u_{lm}^{l+1}(r') . \tag{14}$$

For the corresponding additional potential, we have

$$\mathcal{U}_{self}(r', \vartheta', \varphi') = 4\pi\mathcal{G} \sum_{lm} \frac{1}{2l+1} \left\{ r_b \, (\rho_C - \rho_M) \left(u_r^b\right)_{lm} \left(\frac{r_b}{r'}\right)^{l+1} + r_s \, \rho_M \left(u_r^s\right)_{lm} \left(\frac{r'}{r_s}\right)^{l+1} \right\} Y_{lm}\left(\vartheta', \varphi'\right). \tag{15}$$

The set of partial differential Eqs. (1)–(3) is solved directly in the time domain. We use an extension of the tool described and employed in Tobie et al. (2008) and Běhounková et al. (2015) and implemented by Ondřej Čadek. For the spatial discretization, we use a spherical harmonic decomposition in the lateral directions and a staggered finite difference scheme

in the radial direction. The mantle is decomposed into 95 layers and the maximum degree of spherical harmonic decomposition is set to $l = 5$. For an evaluation of the tidal torque alone it would be sufficient to assume $l = 2$; numerical computation of the tidal heating, however, requires higher values of l. In order to include the self-gravity term correctly, we calculate the memory terms of constitutive Eqs. (3) or (6), and thus the coefficients of u_r as well, iteratively in each time step. The time scheme is described in "Appendix A." Depending on the considered viscosity, we evaluate the tidal torque and the tidal dissipation hundred or thousand times per orbit. Typical timestep for the model planet described in Table 1 is therefore $\Delta t = 10^{-3}$ or $\Delta t = 10^{-4}$ years.

Additionally, before we start the computation itself, it is necessary to choose an appropriate set of initial conditions. The time integration is then performed from these conditions until a relaxed solution is found. We consider the solution as relaxed when the changes in the average tidal dissipation or tidal torque over one orbital period become negligible (see Běhounková et al. 2010). Naturally, our desire is to choose such set of initial strains and stresses, from which the relaxed solution is found as fast as possible. We seek the suitable initial conditions by analyzing the tidal potential. Each mode of the tidal potential consists of two parts: the first, which is constant in time, and the second, with short-term or long-term variations in the orbit (compare with the Fourier series of Kaula 1964). Under our assumption of zero obliquity, the zonal modes ($m = 0$) always involve a nonzero constant term due to the gravitational field of the host star and the centrifugal acceleration caused by the planetary rotation. The sectoral modes ($m = l$), on the other hand, are generally strictly time dependent and their constant term becomes nonzero only in the spin-orbit resonances.

For this reason and in order to improve the rate of convergence of the solution, two kinds of initial conditions were used for our computations. Outside of the spin-orbit resonances we assume that the coefficients of sectoral modes for both the deformation and the internal stresses are initially zero. When considering a tidally locked planet or the zonal modes, however, we first precompute a fast converging "fluid limit," i.e., the relaxed shape and stresses corresponding to a low-viscosity body influenced solely by the constant part of the tidal potential. The computation for the actual viscosity then proceeds from these results, which naturally include nonspherical shape of the body—a hydrostatical shape acquired under the constant part of the potential.

With the stress and strain tensors converged and given, we may proceed to the computation of tidal heating and tidal torque. The average rate of tidal dissipation over a time interval T is computed as

$$P = \frac{1}{T} \int_V \int_t^{t+T} \dot{\varepsilon}(\tau) : \mathbf{D}(\tau) \, d\tau \, dV, \tag{16}$$

where V represents the volume of the planetary mantle and $\dot{\varepsilon}$ is the strain rate tensor. Only in a special case of the Maxwell rheology we may compute the dissipation rate directly as (see e.g., Hanyk et al. 2005)

$$P = \frac{1}{T} \int_V \int_t^{t+T} \frac{\mathbf{D}(\tau) : \mathbf{D}(\tau)}{2\eta} \, d\tau \, dV. \tag{17}$$

To compare the shape of our numerical results with a semi-analytical solution, we re-derive a formula for the tidal heating of a homogeneous spherical body based on Eqs. (10)–(12) of Segatz et al. (1988). Discretizing the time integral and using the Parseval's theorem for the discrete Fourier transform (DFT), one gets

$$P = \frac{5}{8\pi^2} \frac{n_{\text{orb}} \Delta t}{\mathcal{G} r_{\text{s}} N} \int_S \sum_{i=0}^{N-1} \frac{\text{Im}\{\bar{k}_2(\omega_i)\}}{\omega_i} |\xi_i|^2 \, dS, \tag{18}$$

where n_{orb} is the mean motion, ω_i are tidal frequencies, $\bar{k}_2$ is a frequency-dependent complex Love number of degree 2 and ξ_i are DFT coefficients of $\frac{\partial \mathcal{U}_t}{\partial t}$. Time derivatives of the tidal potential are computed numerically with a timestep Δt at N points in the orbit. The complex Love number is defined, e.g., in Castillo-Rogez et al. (2011) in correspondence with the static Love number as

$$\bar{k}_2(\omega) = \frac{3}{2} \frac{\bar{J}(\omega)}{\bar{J}(\omega) + \frac{57}{8\pi \mathcal{G} \rho^2 r_{\text{s}}^2}}, \tag{19}$$

where ρ is the mean density of the planet and $\bar{J}(\omega)$ signifies the complex compliance. Relation (19) is valid as long as we remain in the linear approximation. The compliance of a material described by the Andrade rheology can be expressed as (Castillo-Rogez et al. 2011)

$$\bar{J}(\omega) = \frac{1}{\mu} - \frac{i}{\eta\omega} + \frac{1}{\mu(i\zeta\tau_{\text{M}}\omega)^\alpha} \Gamma(1+\alpha), \tag{20}$$

with $\tau_{\text{M}} = \frac{\eta}{\mu}$ representing the Maxwell time and $\Gamma(x)$ being the Gamma function. The compliance of the Maxwell model is obtained by dropping the last term in the expression.

In order to assess the tidal torque acting on the model planet, we first need to evaluate the disturbing force due to the tidal bulge, i.e., due to the deformation of both upper and lower boundary. At the position of the host star, the disturbing force is given by

$$\mathbf{f}_{\text{dist}}(r, \vartheta_*, \varphi_*) = \sum_{lm} \left[\zeta_{lm}^{\text{b}} \left(\frac{r_{\text{b}}}{r}\right)^{l+2} + \zeta_{lm}^{\text{s}} \left(\frac{r_{\text{s}}}{r}\right)^{l+2} \right] \mathbf{Y}_{lm}^{l+1}(\vartheta_*, \varphi_*), \tag{21}$$

with coefficients

$$\zeta_{lm}^{\text{b}} = 4\pi \sqrt{\frac{l+1}{2l+1}} \mathcal{G} (\rho_{\text{C}} - \rho_{\text{M}}) (u_{\text{r}}^{\text{b}})_{lm} \quad \text{and} \quad \zeta_{lm}^{\text{s}} = 4\pi \sqrt{\frac{l+1}{2l+1}} \mathcal{G} \rho_{\text{M}} (u_{\text{r}}^{\text{s}})_{lm}. \tag{22}$$

The tidal torque acting on a unit mass of the planet due to the star at a distance $\mathbf{r}$ is then

$$\mathcal{T} = \mathbf{r} \times \mathbf{f}_{\text{dist}}. \tag{23}$$

We apply the model on an Earth-size terrestrial planet orbiting a low-mass star (see Table 1) and study the tidal effects as a function of the eccentricity, the mantle viscosity, the spin-orbit ratio and the rheological model.

3 Tidal torque

Evolution of the planetary spin rate is driven by the tidal torque, given by Eq. (23). This torque causes the planet rotation to decelerate when negative and to accelerate when positive. A long-term stability of the spin state requires zero average tidal torque and a distinct shape of its dependence on the spin-orbit ratio (see Figs. 1, 2): The function is above zero to the left from the stable state and below zero to the right. We employ the numerical model to compute the secular tidal torque acting on a deformed planetary body with a highly eccentric orbit ($e = 0.4$). The choice of this particular eccentricity is motivated by a qualitative comparison of our results with the analytical study of Correia et al. (2014).

Table 1 Model parameters

Parameter	Definition	Value
a	Semi-major axis	0.1 AU
e	Eccentricity	0.0–0.5
M_*	Mass of the host star	0.1 solar mass
ρ_M	Density of the mantle	5000 kg m^{-3}
ρ_C	Density of the liquid outer core	9000 kg m^{-3}
ρ_I	Density of the inner core	12,000 kg m^{-3}
r_s	Planetary radius	6370 km
r_b	Radius of the core-mantle boundary	2480 km
r_I	Inner core radius	1200 km
μ	Mantle rigidity	200 GPa
η	Mantle viscosity	10^{14}–10^{24} Pa s
α	Parameter of the Andrade model	0.3
ζ	Parameter of the Andrade model	1

Figure 1 shows the frequency dependence of the average tidal torque for a body described by the Maxwell rheology, Fig. 2 is the average torque for the Andrade rheology. Individual plots illustrate distinct rheological regimes of the planet, given by the mantle viscosity and the orbital period, which is held constant at $T_{orb} = 0.1$ years. The two different sets of viscosities were chosen in order to evaluate the tidal effects in a broad range of realistic terrestrial exoplanets. While the tidal viscosity in the Andrade model could be identified with the same parameter in the mantle convection problems, the viscosity in the Maxwell model should be understood rather as an effective value for the tidal deformation, which correctly predicts the tidal heating in rocky bodies, mimicking the dissipation in the Andrade model (Běhounková et al. 2010, 2013). The effective tidal viscosity is introduced as a frequency-dependent quantity and in the case of terrestrial planets loaded at high frequencies is up to few orders lower than the standard viscosity. Here, we neglect its frequency dependence and consider it as a parameter.

The first picture (upper left corner on both figures) represents the low-viscosity regime ($\eta = 1.4 \times 10^{16}$ Pa s) with only one stable spin state. Such a system would evolve toward pseudo-synchronization, as predicted by the constant time lag theories (Darwin 1880; Alexander 1973; Mignard 1979; Ferraz-Mello et al. 2008), with spin-orbit ratio given by $\frac{\Omega}{n} = 1 + 6e^2 + O(e^4)$. When we increase the viscosity of the mantle, the shape of the function becomes more complex and multiple stable spin states arise, associated with the spin-orbit resonances. This pattern is consistent with predictions of rheologically motivated analytical studies, such as Ferraz-Mello (2013), Correia et al. (2014) and Ferraz-Mello (2015). Finally, in a purely elastic case, the average tidal torque would be zero for every rotational frequency.

The general trend of the tidal torque is similar for both rheological models. However, as is shown, e.g., in Figure 1 of Efroimsky (2012), once we are above a characteristic frequency threshold, determined by the rheological parameters, the decrease in the dissipation rate with increasing tidal frequency (or, alternatively, with increasing viscosity) is slower for the Andrade rheology than for the Maxwell rheology. The dissipation in an Andrade body with given viscosity therefore corresponds to the dissipation in a Maxwell body with lower
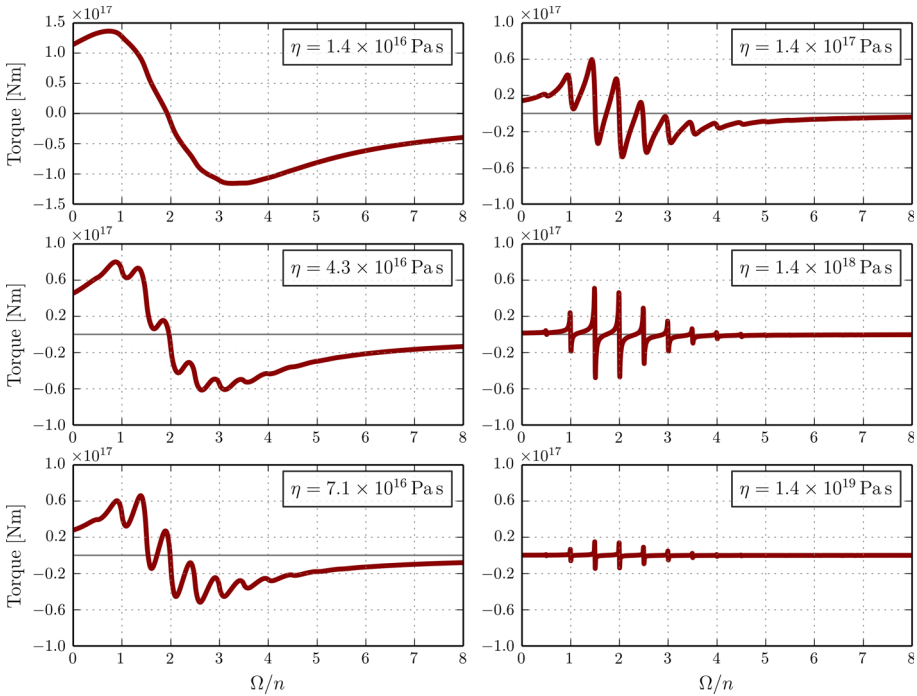
Fig. 1 Average tidal torque as a function of the spin-orbit ratio for six different viscosities in the Maxwell rheological model. The orbital eccentricity was set to $e = 0.4$ (cf. Correia et al. 2014)

viscosity, and this difference becomes prominent especially in the high-viscosity cases. From comparison of Figs. 1 and 2, we may also see that the secular Andrade torque at higher spin-orbit ratios tends to zero much more gradually than its Maxwellian counterpart.

4 Tidal heating

Conclusions of the previous section can be compared with the spin-orbit ratio dependence of average tidal heat rate, depicted in Figs. 3 and 4. For the sake of consistency, we keep the high eccentricity of the orbit, i.e., $e = 0.4$, constant orbital period, $T_{\text{orb}} = 0.1$ years, and the same range of viscosities for both models. The most striking feature of the figures is a significant difference between the magnitude of tidal heating in the Maxwell and the Andrade model at high frequencies (high spin-orbit ratios). While the average power computed in the Maxwell model tends to decline at high rotation rates (the planet operates close to the elastic regime), the power produced in the Andrade model continues to rise and acquires values much higher than observed around the synchronous rotation ($\Omega/n = 1$). The overall shape of the spin-orbit ratio dependence of tidal heating in the Andrade case remains similar for all mantle viscosities.

Another distinction between the two models lies in the shape of local minima. Similarly to the tidal torque with its sole stable spin state at low viscosity, there is only one local minimum in the viscous regime ($\eta = 1.4 \times 10^{16}$ Pa s) and multiple minima elsewhere, typically associated with low spin-orbit resonances. The local minima of the Maxwell model
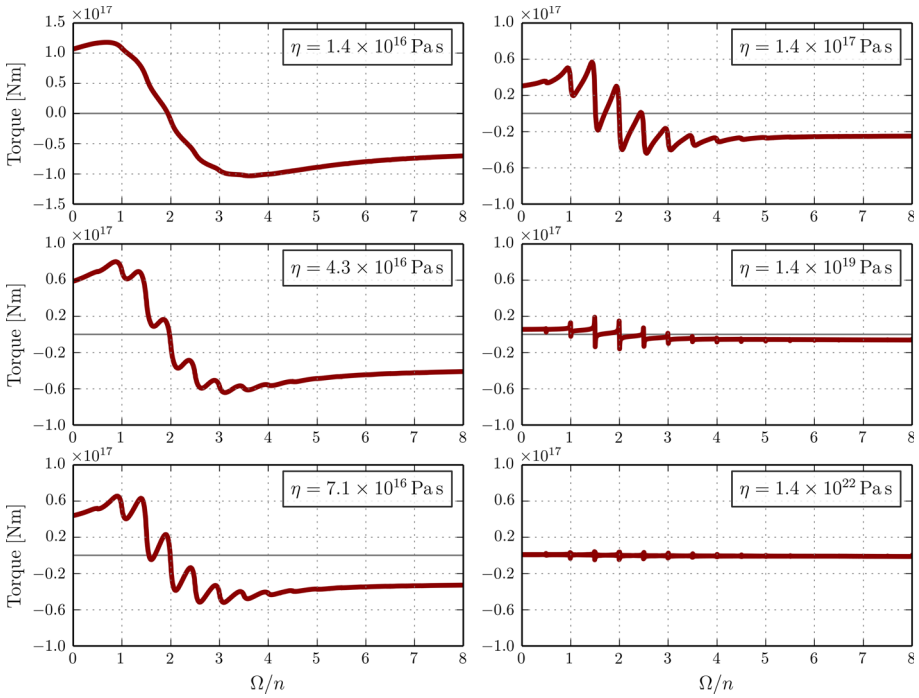
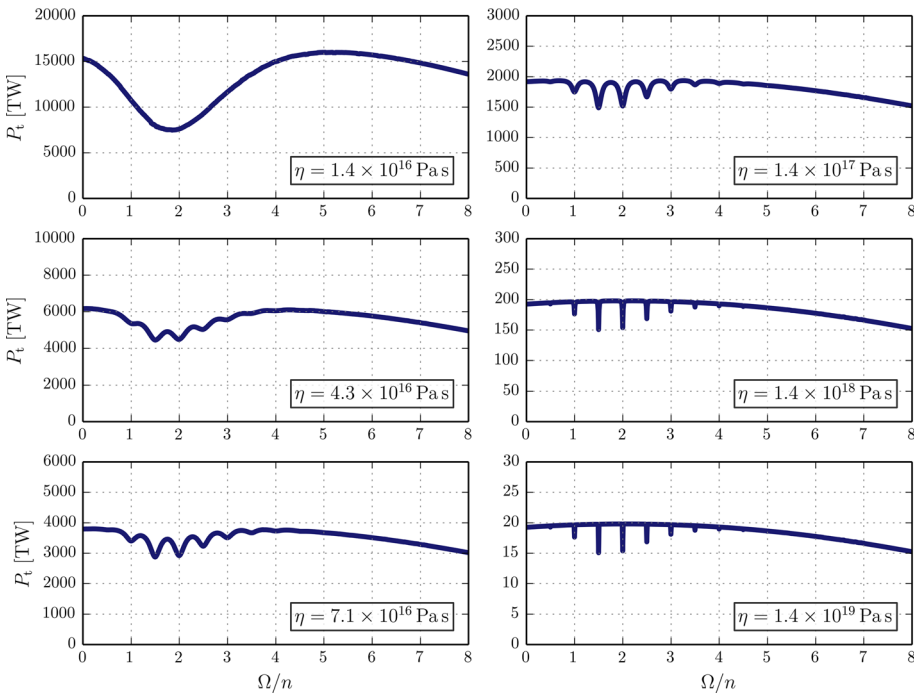**Fig. 2** Average tidal torque in the Andrade rheological model. The orbital eccentricity was set to $e = 0.4$

Fig. 3 Average tidal heating of the model planet presented in Fig. 1, Maxwell model, $e = 0.4$
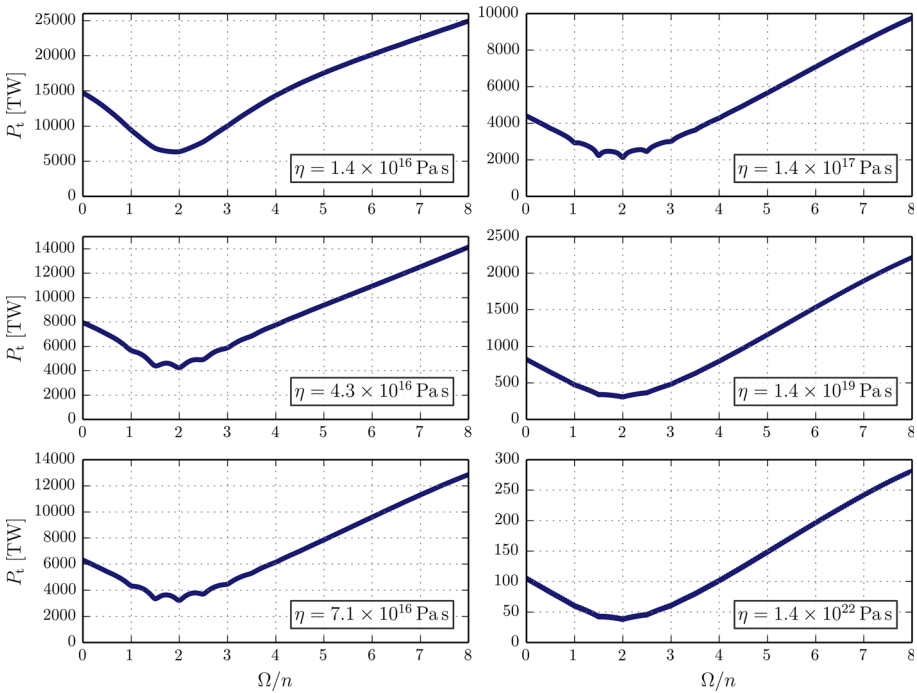
Fig. 4 Average tidal heating of the model planet presented in Fig. 2, Andrade model, $e = 0.4$

get gradually deeper and narrower as we increase the viscosity of the mantle and their depths differ, depending on the orbital eccentricity (Fig. 5). In the Andrade model, on the other hand, local minima remain shallow and broad, disappearing eventually at high mantle viscosities ($\eta > 1.4 \times 10^{19}$ Pa s). Further increase in viscosity ($\eta = 1.4 \times 10^{22}$ Pa s) leads the planet close to the elastic regime with only one global minimum, similar to the global minimum in viscous regime.

At this point we shall note that the planet on eccentric orbit is tidally loaded at a range of frequencies, and while it responds as an elastic body at one frequency, it can still be far from elasticity at another frequency. The terms "elastic" or "viscous" regime, which we use throughout this study, refer to the highest or the lowest value of considered mantle viscosities (see Table 1). A purely elastic body would, in reality, dissipate no energy, independently of the spin-orbit ratio.

A detailed picture of the tidal heating at low spin-orbit ratios (bounded by the 1:1 and the 5:2 spin-orbit resonance) is presented in Figs. 5 and 6. Here, we compare the results for six orbital eccentricities ranging from $e = 0$ to $e = 0.5$ and three different viscosities in both rheological models: 10^{16}, 10^{18} and 10^{20} Pa s in the Maxwell model and 10^{16}, 10^{20} and 10^{24} Pa s in the Andrade model. In the viscous regime ($\eta = 10^{16}$ Pa s) and at low spin-orbit ratios, the Andrade rheology is well approximated by the Maxwell model and the results therefore coincide. Here, we see that the position of the sole local minimum depends on the orbital eccentricity—it tends to higher spin-orbit ratios with more eccentric orbit.

As was mentioned before, the multiple local minima of Maxwell model occur around the spin-orbit resonances. The relative depths of these minima depend on the orbital eccentricity, with the deepest minimum located at the 1:1 spin-orbit resonance of a circular orbit. It
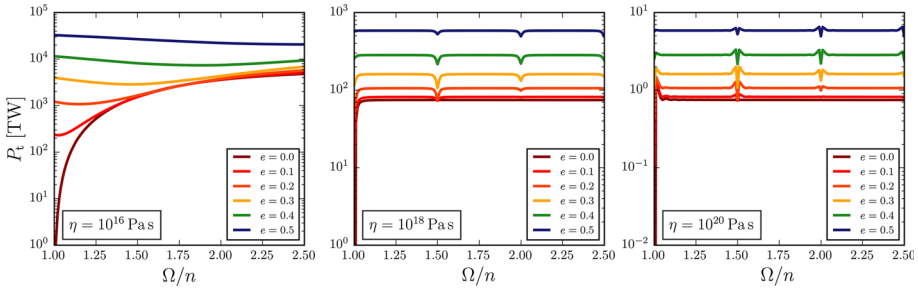
Fig. 5 Average tidal heating as a function of the spin-orbit ratio computed for the Maxwell rheology. Comparison of tidal heat flow for three different viscosities and six eccentricities
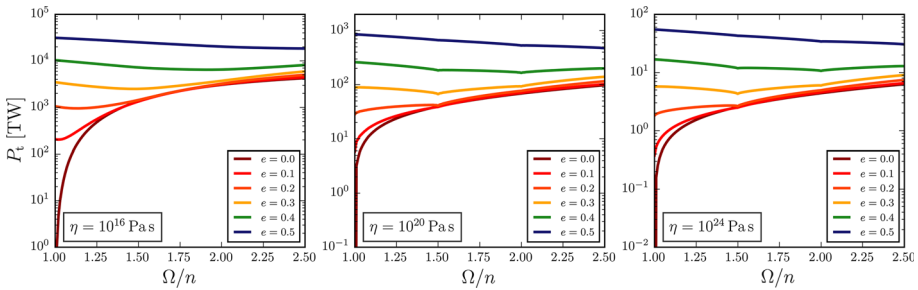

Fig. 6 Average tidal heating as a function of the spin-orbit ratio computed for the Andrade rheology. Comparison of tidal heat flow for three different viscosities and six eccentricities

is clear that the synchronously rotating, zero eccentricity planet exhibits no tidal heating, independently on the viscosity, as it remains locked in its sole stable spin state. Generally, the depth of the minima at higher spin-orbit resonances (2:1, 5:2) increases with increasing eccentricity, while the depth of the minima associated with lower resonances (1:1, 3:2) decreases. The tidal heating computed for the Andrade model with higher viscosities follows a functional dependence on the spin-orbit ratio that is very similar to the viscous regime, including the position of the global minimum. The local minima remain broad and shallow for each of the considered eccentricities.

5 Love numbers

The additional potential $\delta \mathcal{U}$ due to tidal distortions is related to the tide-raising potential $\mathcal{U}$ via Love number k. In a static case, which is treated as fiducial in the standard theories (Kaula 1964; Mignard 1979), the Love number of the l-th mode is a real number, defined as

$$k_l = \frac{\delta U_l}{U_l}, \tag{24}$$

where both potentials are evaluated at the surface of nonrotating planet. Each Love number could be equipped with a phase lag or a time lag, mimicking the overall lagging of the rotating physical body. Choice of a particular frequency dependence (or independence) of the phase lag determines the rheology of the planet.
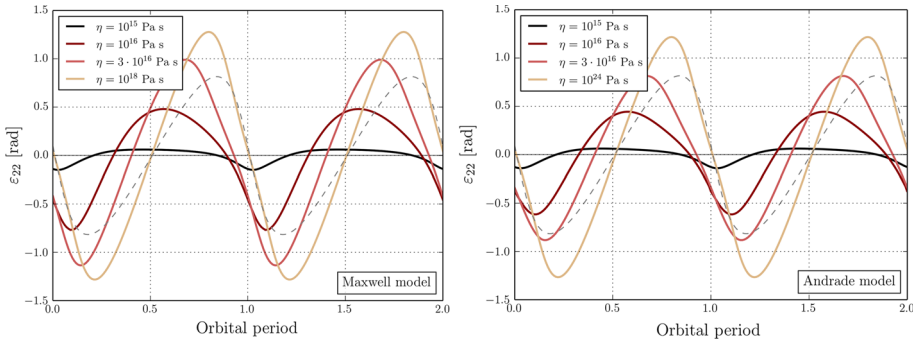
Fig. 7 Variations of the tidal phase lag $\varepsilon_{22}(t)$ as a function of the mantle viscosity for a model with fixed orbital eccentricity $e = 0.4$. *Dashed line* indicates planetograhic longitude of substellar point

Here, we compute the Love numbers in the time domain as

$$k_{lm}(t) = \frac{\delta v_{lm}(t)}{v_{lm}(t)} = |k_{lm}(t)|e^{-i\varepsilon_{lm}(t)}, \tag{25}$$

with $v_{lm}(t)$ and $\delta v_{lm}(t)$ being the spherical harmonic coefficients of the overall potential $\mathcal{U}$ and of the additional potential $\mathcal{U}_{\text{self}}$, respectively, both evaluated at the surface. The phase $\varepsilon_{lm}(t)$ is an angle between the symmetry axes of the two potentials in the time domain. When the order m is nonzero, the coefficients of the potentials are complex, rendering a complex-valued $k_{lm}(t)$ as well. In this special case and considering loading of the mode (l, m) only on one frequency (e.g., a nonsynchronously rotating planet on a circular orbit), the phase $\varepsilon_{lm}(t)$ coincides with the phase lag between the tidal and the additional potential, as traditionally defined in the frequency domain (e.g., Kaula 1964). To illustrate the tidal deformation in the two rheological models considered here, we plot the Love numbers $k_{22}(t)$ and $k_{20}(t)$ for two different orbital eccentricities and spin states.

Our first toy-model is a synchronously rotating planet on an eccentric orbit with $e = 0.4$. We evaluate the quantities mentioned above, assuming that the planet behaves either as a Maxwell body with effective viscosities between 10^{15} and 10^{18} Pa s or as an Andrade body with viscosities ranging from 10^{15} to 10^{24} Pa s. Other parameters, including the rigidity of the mantle, are kept constant. Figure 7 shows time variations of the tidal phase lag ε_{22}. The tidal deformation in a viscous regime ($\eta = 10^{15}$ Pa s) is properly described by a constant time lag model (e.g., Darwin 1880; Mignard 1979; Correia and Laskar 2010), which prescribes the phase lag as a linear function of the loading frequency. The instantaneous angular velocity of the disturbing body on the planet's sky, in our case, is related to the time derivative of the true anomaly v,

$$\text{freq.} = \Omega_{\text{rot}} - \frac{dv}{dt}, \tag{26}$$

and this gives the low-viscosity phase lag the shape of its time dependence (black curve in Fig. 7).

A characteristic feature arises also in the high-viscosity regime, where the relaxation time gets long compared to the orbital period. Here, we initiate the computations in a "fluid limit." The "fluid" tidal bulge, corresponding to the constant part of the tidal potential, virtually freezes at the zero longitude, resulting in a periodically changing nonzero tidal lag (and nonzero instantaneous tidal torque), which follows the geometric libration of the planet. The phase lag is therefore zero, when the planet resides in the periapsis or apoapsis,
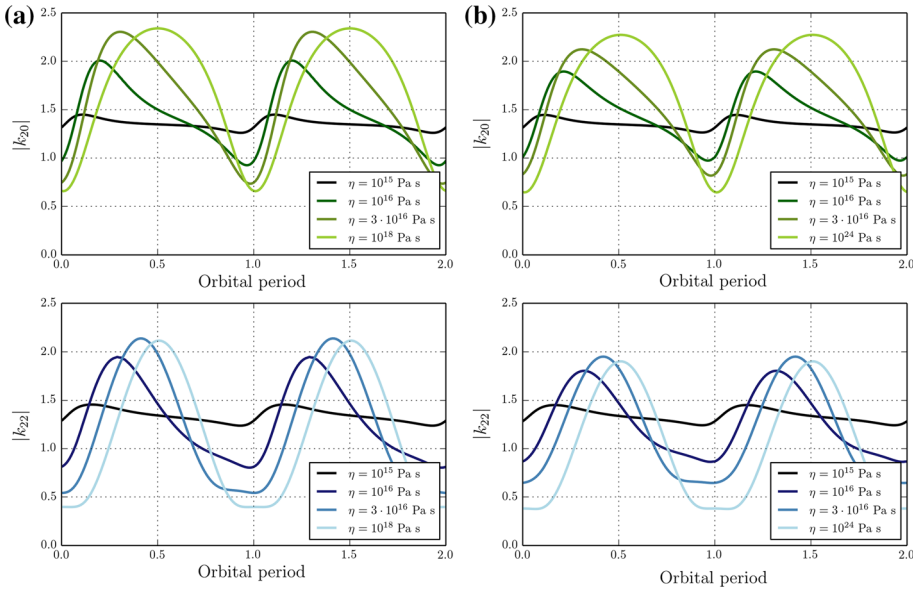
Fig. 8 Variations of the magnitude of potential Love numbers $|k_{20}(t)|$ and $|k_{22}(t)|$ as a function of mantle viscosity

and—if there were no other components to the tidal bulge—would attain a maximum value of approximately $2 \arcsin e$ (that is ≈ 0.8 in our case, dashed line in Fig. 7) at a planet–star distance $r = a \sqrt[4]{(1 - e^2)}$ (Dobrovolskis 2007). Another, nonconstant parts of the tidal potential excite the mantle on a variety of frequencies, resulting in an overall tidal lag which differs from the prescribed value and which is here plotted in tan color.

Figure 8 presents the time variations of the magnitudes of the Love numbers $k_{20}(t)$ and $k_{22}(t)$ for the Maxwell (left column) and the Andrade (right column) rheology. Again, we may see that the time variations are small for the viscous limit, when the planet almost perfectly complies with the changing tidal potential, and are large in the high-viscosity regime, when the planet acts like a rigid body. Furthermore, we may see that the mean value of both Love numbers in the low-viscosity case is close to the fluid limit $k = 1.5$. When we increase the viscosity, the relaxation time of the mantle increases as well and it becomes longer than the loading period. The planet then keeps a permanent shape corresponding to the constant part of the potential. In the periapsis, its deformation is smaller than that of a fluid body subjected to the same tidal potential, and the value of $k_{20}(t)$ and $k_{22}(t)$ is substantially lower than 1.5. In the apoapsis, on the other side, the acquired permanent deformation is larger than would correspond to the tidal potential, and the Love numbers exceed 1.5. The highest viscosity case ($\eta = 10^{18}$ Pa s in the Maxwell model or $\eta = 10^{24}$ Pa s in the Andrade model), plotted in light green and light blue in Fig. 8, confronts us with a time dependence of Love numbers that is driven essentially by the variations of the denominator in (24).

Our second toy-model is a nonsynchronously rotating planet on a circular orbit. In this case, the magnitudes of the Love numbers $k_{20}(t)$ and $k_{22}(t)$ as well as the phase lag $\varepsilon_{22}(t)$ attain a constant value, which is, among other parameters, a function of the tidal frequency and the viscosity. Here, we set the tidal frequency constant ($\Omega/n = 2.1$) and explore the viscosity dependence of the Love number k_{22}. As depicted in Fig. 9, tidal loading may operate in two
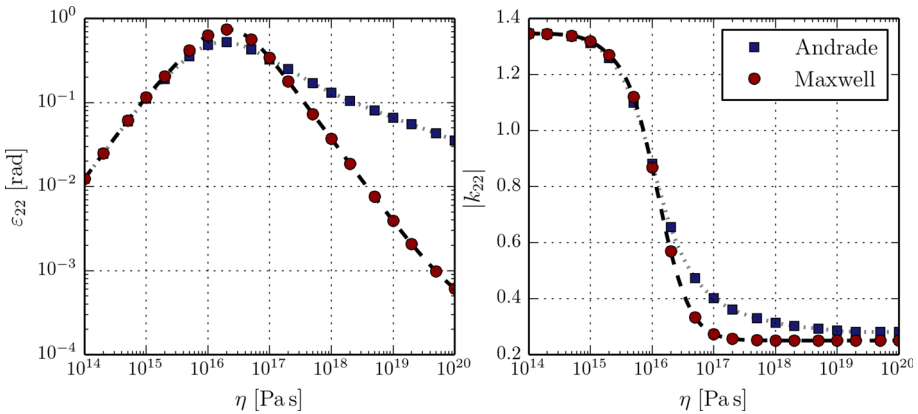
Fig. 9 The phase lag ε_{22} and the Love number $|k_{22}|$ as a function of the mantle viscosity for a planet on circular orbit rotating nonsynchronously with spin-orbit ratio $\Omega/n = 2.1$. *Red dots* indicate the Maxwell rheology, *blue squares* stand for the Andrade rheology

extreme regimes, characterizing the elastic and the viscous limit with a negligible tidal lag, and in a transitional regime, where the tidal lag attains its maximal value (cf. Love numbers in the analytical model of Correia et al. 2014). At higher viscosities the Love numbers, and especially their phase lags, differ substantially for the two rheologies under considerations. The decrease in the phase lag toward the elastic limit is much more gradual in the case of the Andrade rheology than for the Maxwell rheology. Differences in the magnitude of the Love number are less pronounced.

6 Discussion

The thermal and rotational state of close-in exoplanets subjected to significant tidal dissipation is dictated by their orbital elements and the rheological regime. Increase in the orbital eccentricity may enhance the tidal heating by an order of magnitude. Different frequency dependencies of the tidal response in both rheological models in question may lead to a completely different thermal evolution. While a planet governed by the Maxwell rheology attains deep local minima of the tidal heating, associated with the lower spin-orbit resonances, and the dissipation undergone by its interior diminishes as we proceed to higher spin rates, the heat production of a body described by the Andrade model increases with faster rotation and the local minima are observed rather at high spin-orbit resonances. We note that the location and depth of the local minima, as well as the occurence of other tidal effects (e.g., locking into stable spin states), depend not only on the mantle viscosity, but rather on a combination of the viscosity and the tidal frequency. These two parameters together determine the rheological regime of the planet.

The tidal heating depicted in Figs. 3, 4, 5 and 6 would be, in extreme cases, able to melt the entire planetary mantle, leading eventually to a fluid-like behavior. Furthermore, even in a less extreme scenario, the enhanced heat production combined with possible tidal locking and resulting uneven insolation may alter the planet's rheological regime (due to the temperature dependence of viscosity or due to different deformation mechanisms involved in the mantle dynamics) and lead to decrease or further increase in the tidal dissipation. The tidal evolution

of a close-in rocky exoplanet, e.g., its despinning, its thermal history or the rate of orbital evolution, is therefore closely related to its rheological regime, which may, on the contrary, vary with the instantaneous orbital or rotational parameters.

As the tidal heating and the insolation pattern depend on the exact orbital parameters (e.g., Beuthe 2013; Dobrovolskis 2013), the rheological structure of realistic close-in exoplanets may become considerably heterogeneous. Tidal locking into a spin-orbit resonance or, specifically, into the synchronous spin state, also leads to a distinct convection pattern (Běhounková et al. 2010; Gelman et al. 2011; van Summeren et al. 2011). The numerical model described here enables computation of tidal effects also in a planet with generally 3D viscosity structure and with possibly radially dependent rigidity. However, in the present parametric studies, we held the mantle viscosity homogeneous and studied only the effects of its varying magnitude, so that the numerical model could be compared with existing analytical tidal theories. Figure 1, depicting the spin-orbit ratio dependence of tidal torque in the Maxwell model, is intended to be compared qualitatively with Figure 4 of Correia et al. (2014). Similarly, Fig. 9 is identified with Figure 2 of the same paper or with any plot of the dissipation spectrum for the Maxwell and the Andrade rheology (e.g., Castillo-Rogez et al. 2011; Efroimsky 2012; Běhounková et al. 2013).

The characteristic pattern of the average tidal torque and the existence of two distinct regimes—a sole pseudo-synchronous rotation of low-viscosity bodies versus multiple stable spin states of high-viscosity spheres—has already been explored and discussed by the authors of recent analytical tidal models (Correia et al. 2014; Ferraz-Mello 2015). It is worth noting that the rheological regime of the planet is determined not only by its viscosity, but rather by a combination of the viscosity and the excitation frequency. Therefore, even a terrestrial planet may behave as a "fluid" body and a close-in gas giant (a "hot Jupiter") on eccentric orbit may become locked into a nonsynchronous spin-orbit resonance. Both Correia et al. (2014) and Ferraz-Mello (2015) take this into account by introducing a combination of the mean motion and the relaxation time or relaxation factor, which could be related to the mean viscosity of the planet.

Moreover, the number and exact positions of zero points of the average tidal torque are a function of eccentricity. We have particularly presented the case of a highly eccentric orbit with $e = 0.4$. Several other cases, however, can be found in Ferraz-Mello (2015), who studies the stationary spin states for eccentricities ranging from $e = 0$ to $e = 0.5$. The author shows that increase in the eccentricity causes shifting of the sole solution in the low-viscosity case (in concordance with constant time lag models) and increase in the number of solutions in the high-viscosity case. The relative stabilities of particular solutions are affected as well, enabling the prediction of rotation states of moons and planets on eccentric orbits. Ferraz-Mello (2015) also shows that spin-orbit resonances, in contrast to pseudo-synchronous rotation, are not stationary solutions but periodic attractors: a planet on eccentric orbit undergoes physical libration.

In order to compare the numerically obtained tidal heating with a semi-analytical solution, we evaluated the dissipation in a homogeneous sphere subjected to the same tidal potential as in the numerical model. The average heat production due to the tidal dissipation was computed in correspondence with Segatz et al. (1988), where we substituted the frequency independent static Love number k_2 with a set of frequency (and rheology) dependent complex Love numbers, described, e.g., in Castillo-Rogez et al. (2011). This was done for both the Maxwell and the Andrade rheology. Resulting tidal heating of a body with $\eta = 10^{18}$ Pa s is shown in Fig. 10. For the sake of comparison, we also replot Fig. 9 with the addition of semi-analytically obtained Love numbers $|k_2|$ and phase lags ε_2. Here, it is necessary to point out that the planet in the semi-analytical model is considered a homogeneous sphere, dissipating
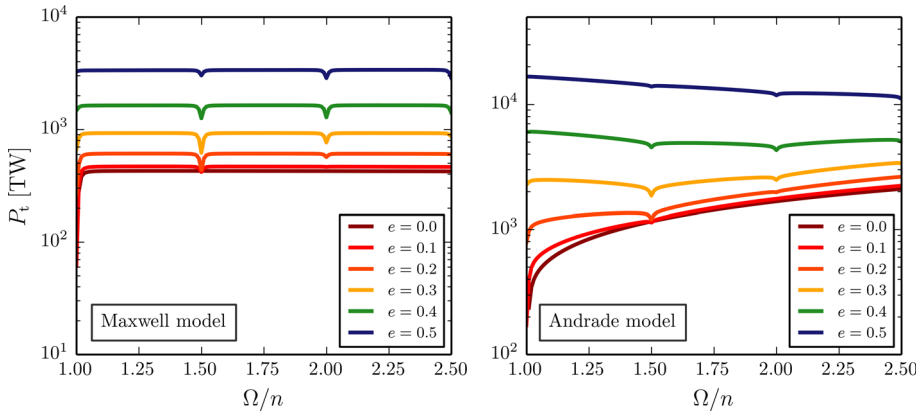
Fig. 10 Average tidal heating computed semi-analytically for $\eta = 10^{18}$ Pa s and both rheological models
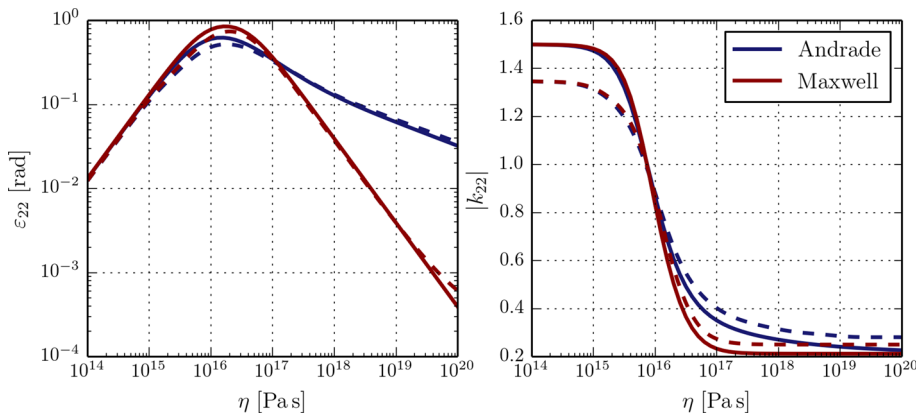

Fig. 11 Comparison of semi-analytical (*solid line*) and numerical (*dashed line*) phase lags and Love numbers for a planet on circular orbit with spin-orbit ratio $\Omega/n = 2.1$

the energy in the entire volume, whereas our numerical model computes the dissipation solely in the mantle. The tidal heating obtained semi-analytically is therefore several times higher than the numerical predictions. The overall shape of the spin rate dependence of tidal heating is, nevertheless, very similar in both approaches, verifying the applicability of our model.

Similarly, the semi-analytical and the numerical Love numbers (Fig. 11) tend to different values at the limits of the viscosity scale. This is naturally caused by the presence of a planetary core. Folonier et al. (2015) and Wahl et al. (2017) predict that for a two-layer core-shell model of a fluid planet the surface flattening is always smaller than would correspond to a homogeneous body. Using Eq. (41) of Folonier et al. (2015) and approximating our solid-liquid core by a single fluid sphere (as we do not consider the deformation of the inner core), we find the theoretical value of the fluid Love number to be $k_f \approx 1.349$. This is close to our numerical result, giving $k_f \approx 1.346$ in the lowest viscosity case ($\eta = 10^{14}$ Pa s). The slight discrepancy can be attributed to different density structure of the core in our study and to the fact that our "lowest viscosity case" is still only an approximation to the real fluid limit.

7 Conclusion

In this paper, we presented a numerical model of tides based on the direct solution of continuum mechanics equations for a disturbed planetary mantle. The model enables computation of tidal deformation and dissipation for generally nonhomogeneous planets governed either by the Maxwell or the Andrade rheology. We then performed a series of calculations, studying the parameter dependence of the tidal heating, the tidal torque and the complex Love numbers. The results for the Maxwell rheology were qualitatively compared to the analytical model of Correia et al. (2014). We also computed the tidal heating semi-analytically, by a method based on Segatz et al. (1988) and Castillo-Rogez et al. (2011).

When describing the tidal response of terrestrial bodies, the Maxwell model is often utilized as a practical substitute for the more complex and more accurate Andrade rheology. Indeed, the two models almost coincide at low viscosities (or low frequencies) and their predictions for the tidal torque and the Love numbers are very similar also in the higher viscosity regimes, as long as we keep the notion of effective tidal viscosities, which can be up to few orders lower than the "standard" viscosities utilized, e.g., in the mantle convection models. The crucial difference between the two rheological models arises in the comparison of spin-orbit ratio dependence of the tidal heating. However, even in this case the Andrade model can be approximated by the Maxwell model—the concept of frequency-dependent effective viscosity remains valid. When computing the tidal evolution or the tidal heating of terrestrial exoplanets, we must remember that only a planet on circular orbit is excited at one sole frequency. Hence, only the dissipation inside planets on circular orbits would be consistently approximated by a single-viscosity Maxwell model. For the eccentric orbits, it would be necessary to find all present frequencies and to sum the tidal heating over multiple Maxwell models, with a variety of effective viscosities. Only after this procedure, we would be able to get Figs. 4 or 6 without using the Andrade model directly.

As was already pointed out by Frouard et al. (2016), the place of numerical models among analytical theories is irreplaceable when dealing with complex rheologies, planets with nontrivial internal structure or nonspherical shape, and with analytically challenging phenomena. While the analytical models provide us with general predictions for the tidal evolution of terrestrial bodies, semi-analytical or numerical models may help us to understand subtle details, given for example by coupling of the orbital (or rotational) and the internal dynamics or by sensitivity of the tidal heating to the chosen rheology.

Appendix A Iterative time scheme

To find the numerical solution of the governing equations, we use and further develop a tool employed in Tobie et al. (2008) and Běhounková et al. (2015), implemented by Ondřej Čadek. We have extended this code to account for a general tidal potential, rotational deformation

and self-gravity. In order to evaluate the tidal torque correctly, we have updated originally explicit time scheme to include the self-gravity and the memory term implicitly.

For the $(i + 1)$-th time step and the explicit time scheme, considering constant time step Δt, Eqs. (1)–(5) are discretized as follows (Běhounková et al. 2015):

Governing equations:

$$\nabla \cdot \mathbf{u}_{i+1} = 0 \tag{27}$$

$$-\nabla \pi_{i+1} + \nabla \cdot \mathbf{D}_{i+1} = \rho_{\mathrm{M}} \left[(\mathbf{f}_{\mathrm{t}})_{i+1} + (\mathbf{f}_{\mathrm{cf}})_{i+1} + (\mathbf{f}_{\mathrm{self}})_i \right]. \tag{28}$$

Constitutive equation:

$$2\varepsilon_{i+1} - \frac{\mathbf{D}_{i+1}}{\mu} = \overbrace{\frac{1}{2} \frac{\mathbf{D}_0}{\eta} \Delta t + \sum_{j=1}^{j=i} \frac{\mathbf{D}_j}{\eta} \Delta t}^{M_i}$$

$$+ \underbrace{\frac{1}{2} w_{(i+1)0} \left(\frac{\mathbf{D}_1}{(\zeta \eta)^\alpha} - \frac{\mathbf{D}_0}{(\zeta \eta)^\alpha} \right) + \sum_{j=1}^{j=i-1} \frac{1}{2} w_{(i+1)j} \left(\frac{\mathbf{D}_{j+1}}{(\zeta \eta)^\alpha} - \frac{\mathbf{D}_{j-1}}{(\zeta \eta)^\alpha} \right)}_{A_i}, \tag{29}$$

where w_{ij} are weights,

$$w_{(i+1)j} = (i + 1 - j)^\alpha \Delta t^\alpha \mu^{\alpha-1}, \tag{30}$$

M_i is the explicit memory term for the Maxwell rheology and A_i is the additional explicit memory term describing the Andrade rheology.

Boundary conditions:

$$(-\pi_{i+1}\mathbf{I} + \mathbf{D}_{i+1}) \cdot \mathbf{e}_{\mathrm{r}} - \left(u_{\mathrm{r}}^{\mathrm{s}} \right)_{i+1} \rho_{\mathrm{M}} \mathbf{g}_{\mathrm{s}} = 0, \tag{31}$$

$$(-\pi_{i+1}\mathbf{I} + \mathbf{D}_{i+1}) \cdot \mathbf{e}_{\mathrm{r}} + \left(u_{\mathrm{r}}^{\mathrm{b}} \right)_{i+1} (\rho_{\mathrm{C}} - \rho_{\mathrm{M}}) \mathbf{g}_{\mathrm{b}} = -\rho_{\mathrm{C}} \left[(\mathcal{U}_{\mathrm{t}})_{i+1} + (\mathcal{U}_{\mathrm{cf}})_{i+1} + (\mathcal{U}_{\mathrm{self}})_i \right] \mathbf{e}_{\mathrm{r}}. \tag{32}$$

The initial step ($l = 0$) in the iterative scheme is determined explicitly. For the lth ($l \geq 1$) iteration, we then have

Governing equations:

$$\nabla \cdot \mathbf{u}_{i+1} = 0 \tag{33}$$

$$-\nabla \pi_{i+1} + \nabla \cdot \mathbf{D}_{i+1} = \rho_{\mathrm{M}} \left[(\mathbf{f}_{\mathrm{t}})_{i+1} + (\mathbf{f}_{\mathrm{cf}})_{i+1} + (\mathbf{f}_{\mathrm{self}})_{i+1}^{l-1} \right]. \tag{34}$$

Constitutive equation:

$$2\varepsilon_{i+1} - \frac{\mathbf{D}_{i+1}}{\mu} = M_i + \frac{1}{2} \frac{\mathbf{D}_{i+1}^{l-1}}{\eta} \Delta t + A_i + \frac{1}{4} w_{(i+1)i} \left(\frac{\mathbf{D}_{i+1}^{l-1}}{(\zeta \eta)^\alpha} - \frac{\mathbf{D}_{i-1}}{(\zeta \eta)^\alpha} \right). \tag{35}$$

Boundary conditions:

$$(-\pi_{i+1}\mathbf{I} + \mathbf{D}_{i+1}) \cdot \mathbf{e}_r - \left(u_r^s\right)_{i+1} \rho_M \mathbf{g}_s = 0, \tag{36}$$

$$(-\pi_{i+1}\mathbf{I} + \mathbf{D}_{i+1}) \cdot \mathbf{e}_r + \left(u_r^b\right)_{i+1} (\rho_C - \rho_M) \mathbf{g}_b = -\rho_C \left[(\mathcal{U}_t)_{i+1} + (\mathcal{U}_{cf})_{i+1} + (\mathcal{U}_{self})_{i+1}^{l-1} \right] \mathbf{e}_r. \tag{37}$$

The iteration is repeated until $\frac{|\mathbf{D}_{II}^l - \mathbf{D}_{II}^{l-1}|}{\mathbf{D}_{II}^l} < \epsilon$, where we usually assume $\epsilon = 10^{-4}$.

Appendix B Spherical harmonics

Any quadratically integrable scalar function f of spherical coordinates ϑ and φ can be expressed as a linear combination of surface spherical harmonics Y_{lm} (see e.g., Varshalovich et al. 1988)

$$f(\vartheta, \varphi) = \sum_{l=0}^{\infty} \sum_{m=-l}^{l} f_{lm} Y_{lm}(\vartheta, \varphi) \tag{38}$$

with coefficients

$$f_{lm} = \int_0^{2\pi} \int_0^{\pi} f(\vartheta, \varphi) \bar{Y}_{lm}(\vartheta, \varphi) \sin \vartheta \, d\vartheta \, d\varphi. \tag{39}$$

We introduce the spherical harmonics as

$$Y_{lm}(\vartheta, \varphi) = (-1)^m \mathcal{N}_{lm} \mathcal{P}_{lm}(\cos \vartheta) e^{im\varphi}, \tag{40}$$

where $\mathcal{N}_{lm}$ is the normalization factor

$$\mathcal{N}_{lm} = \sqrt{\frac{(2l+1)(l-m)!}{4\pi(l+m)!}}, \tag{41}$$

and $\mathcal{P}_{lm}(\cos \vartheta)$ are fully normalized associated Legendre polynomials of degree l and order m. Spherical harmonics represent a complete set of orthonormal functions on the surface of a sphere, with the orthonormality relation given by

$$\int_0^{2\pi} \int_0^{\pi} Y_{l_1 m_1}(\vartheta, \varphi) \bar{Y}_{l_2 m_2}(\vartheta, \varphi) \sin \vartheta \, d\vartheta \, d\varphi = \delta_{l_1 l_2} \delta_{m_1 m_2}. \tag{42}$$

The notion of spherical harmonic decomposition can be generalized to account for the vector and tensor functions as well. Vector spherical harmonics are introduced as

$$\mathbf{Y}_{lm}^k(\vartheta, \varphi) = \sum_{\mu=-1}^{+1} \sum_{\nu=-k}^{k} C_{k\nu 1\mu}^{lm} Y_{k\nu} \mathbf{e}_\mu, \tag{43}$$

with $C_{k\nu 1\mu}^{lm}$ being the Clebsch–Gordan coefficients and $\mathbf{e}_\mu$ being the components of a basis which appropriately follows the pattern of Y_{lm} under rotations. They are related to the cartesian basis vectors $\{\mathbf{e}_x, \mathbf{e}_y, \mathbf{e}_z\}$ by

$$\mathbf{e}_{-1} = \frac{1}{\sqrt{2}} \left(\mathbf{e}_x - i\,\mathbf{e}_y \right),$$

$$\mathbf{e}_0 = \mathbf{e}_z, \tag{44}$$

$$\mathbf{e}_1 = -\frac{1}{\sqrt{2}} \left(\mathbf{e}_x + i\,\mathbf{e}_y \right).$$

Finally, we define the tensor spherical harmonics

$$\mathbf{Y}_{lm}^{kn}(\vartheta, \varphi) = \sum_{\mu=-1}^{+1} \sum_{\nu=-k}^{k} \mathcal{C}_{k\nu n\mu}^{lm} Y_{k\nu}\, \mathbf{e}_{n\mu}, \tag{45}$$

with a basis

$$\mathbf{e}_{j\lambda} = \sum_{\nu,\mu} \mathcal{C}_{1\nu 1\mu}^{j\lambda}\, \mathbf{e}_\nu \otimes \mathbf{e}_\mu, \tag{46}$$

where $\otimes$ symbolizes a dyadic product.

References

Alexander, M.E.: The weak friction approximation and tidal evolution in close binary systems. Astrophys. Space Sci. **23**(2), 459–510 (1973)

Barnes, R., Jackson, B., Greenberg, R., Raymond, S.N.: Tidal limits to planetary habitability. Astrophys. J. Lett. **700**(1), L30–L33 (2009)

Běhounková, M., Tobie, G., Choblet, G., Čadek, O.: Coupling mantle convection and tidal dissipation: applications to Enceladus and earth-like planets. J. Geophys. Res.: Planets **115**(E9) (2010). doi:10.1029/2009JE003564

Běhounková, M., Tobie, G., Choblet, G., Čadek, O.: Impact of tidal heating on the onset of convection in Enceladus's ice shell. Icarus **226**(1), 898–904 (2013)

Běhounková, M., Tobie, G., Čadek, O., Choblet, G., Porco, C., Nimmo, F.: Timing of water plume eruptions on Enceladus explained by interior viscosity structure. Nat. Geosci. **8**(8), 601–604 (2015)

Beuthe, M.: Spatial patterns of tidal heating. Icarus **223**(1), 308–329 (2013)

Boué, G., Correia, A.C.M., Laskar, J.: Complete spin and orbital evolution of close-in bodies using a Maxwell viscoelastic rheology. Celest. Mech. Dyn. Astron. **126**(1–3), 31–60 (2016)

Castillo-Rogez, J.C., Efroimsky, M., Lainey, V.: The tidal history of Iapetus: spin dynamics in the light of a refined dissipation model. J. Geophys. Res.: Planets **116**(E9) (2011). doi:10.1029/2010JE003664

Correia, A., Laskar, J.: Tidal evolution of exoplanets. arXiv:1009.1352v2 (2010)

Correia, A.C.M., Boué, G., Laskar, J., Rodríguez, A.: Deformation and tidal evolution of close-in planets and satellites using a Maxwell viscoelastic rheology. Astron. Astrophys. **571**, A50 (2014)

da Andrade, E.N.C.: On the viscous flow in metals and allied phenomena. Proc. R. Soc. A Math. Phys. **84**(567), 1–12 (1910)

Darwin, G.H.: On the secular change in the elements of the orbit of a satellite revolving about a tidally distorted planet. Philos. Trans. R. Soc. **171**, 713–891 (1880). **(repr. in Scientific Papers, Cambridge, Vol. II, 1908)**

Dobrovolskis, A.R.: Spin states and climates of eccentric exoplanets. Icarus **192**(1), 1–23 (2007)

Dobrovolskis, A.R.: Insolation on exoplanets with eccentricity and obliquity. Icarus **226**(1), 760–776 (2013)

Efroimsky, M.: Tidal dissipation compared to seismic dissipation: in small bodies, earths and super-earths. Astrophys. J. **746**(2), 150 (2012)

Efroimsky, M., Lainey, V.: Physics of bodily tides in terrestrial planets and the appropriate scales of dynamical evolution. J. Geophys. Res.: Planets **112**(E12) (2007). doi:10.1029/2007JE002908

Ferraz-Mello, S.: Tidal synchronization of close-in satellites and exoplanets. A rheophysical approach. Celest. Mech. Dyn. Astron. **116**(2), 109–140 (2013)

Ferraz-Mello, S.: Tidal synchronization of close-in satellites and exoplanets: II. Spin dynamics and extension to Mercury and exoplanet host stars. Celest. Mech. Dyn. Astron. **122**(4), 359–389 (2015)

Ferraz-Mello, S., Rodríguez, A., Hussmann, H.: Tidal friction in close-in satellites and exoplanets. The Darwin theory re-visited. Celest. Mech. Dyn. Astron. **101**(1–2), 171–201 (2008)

Folonier, H.A., Ferraz-Mello, S., Kholshevnikov, K.V.: The flattenings of the layers of rotating planets and satellites deformed by a tidal potential. Celest. Mech. Dyn. Astron. **122**(2), 183–198 (2015)

Frouard, J., Quillen, A.C., Efroimsky, M., Giannella, D.: Numerical simulation of tidal evolution of a viscoelastic body modeled with a mass-spring network. Mon. Not. R. Astron. Soc. **458**(3), 2890–2901 (2016)

Gelman, S.E., Elkins-Talton, L.T., Seager, S.: Effects of stellar flux on tidally locked terrestrial planets: degree-1 mantle convection and local magma ponds. Astrophys. J. **735**(2), 72 (2011)

Gerstenkorn, H.: Über Gezeitenreibung beim Zweikörperproblem. Z. Astrophys. **36**, 245–275 (1955)

Goldreich, P.: Final spin states of planets and satellites. Astron. J. **71**, 1 (1966)

Goldreich, P., Soter, S.: Q in the solar system. Icarus **5**(1), 375–389 (1966)

Hanyk, L., Matyska, C., Yuen, D.A.: Short time-scale heating of the Earth's mantle by ice-sheet dynamics. Earth Planets Space **57**(9), 895–902 (2005)

Helmert, F.R.: Die mathematischen und physikalischen theorieen der höheren geodäsie. II. Teil: Die physikalischen Theorieen. B. G. Teubner, Leipzig (1884)

Henning, W.G., O'Connell, R.J., Sasselov, D.D.: Tidally heated terrestrial exoplanets: viscoelastic response models. Astrophys. J. **707**(2), 1000–1015 (2009)

Hut, P.: Tidal evolution in close binary systems. Astron. Astrophys. **99**(1), 126–140 (1981)

Kaula, W.M.: Analysis of gravitational and geometric aspects of geodetic utilization of satellites. Geophys. J. R. Astron. Soc. **5**(2), 104–133 (1961)

Kaula, W.M.: Tidal dissipation by solid friction and the resulting orbital evolution. Rev. Geophys. **2**(4), 661–685 (1964)

Kjartansson, E.: Constant Q-wave propagation and attenuation. J. Geophys. Res. Solid Earth **84**(B9), 4737–4748 (1979)

MacDonald, G.J.F.: Tidal friction. Rev. Geophys. **2**(3), 467–541 (1964)

Makarov, V.V., Efroimsky, M.: No pseudosynchronous rotation for terrestrial planets and moons. Astrophys. J. **764**(1), 27 (2013)

Mayor, M., Queloz, D.: A Jupiter-mass companion to a solar-type star. Nature **378**(6555), 355–359 (1995)

McCarthy, C., Goldsby, D.L., Cooper, R.F.: Transient and steady-state creep responses of ice-I/magnesium sulfate hydrate Eutectic aggregates. In: Proceedings of the 38th Lunar and Planetary Science Conference, (Lunar and Planetary Science XXXVIII), held March 12–16, 2007 in League City, Texas. LPI Contribution No. 1338, p. 2429 (2007)

Mignard, F.: The evolution of the lunar orbit revisited I. Moon Planets **20**(3), 301–315 (1979)

Mullally, F., Coughlin, J.L., Thompson, S.E., et al.: Planetary candidates observed by Kepler. VI. Planet sample from Q1–Q16 (47 Months). Astrophys. J. Suppl. **217**(2), 31 (2015)

Néron de Surgy, O., Laskar, J.: On the long term evolution of the spin of the Earth. Astron. Astrophys. **318**, 975–989 (1997)

Segatz, M., Spohn, T., Ross, M.N., Schubert, G.: Tidal dissipation, surface heat flow, and figure of viscoelastic models of Io. Icarus **75**(2), 187–206 (1988)

Singer, S.F.: The origin of the Moon and geophysical consequences. Geophys. J. R. Astron. Soc. **15**(1–2), 205–226 (1968)

Souček, O., Hron, J., Běhounková, M., Čadek, O.: Effect of the tiger stripes on the deformation of Saturn's moon Enceladus. Geophys. Res. Lett. **43**(14), 7417–7423 (2016)

Tan, B.H., Jackson, I., Fitz Gerald, J.D.: Shear wave dispersion and attenuation in fine-grained synthetic olivine aggregates: preliminary results. Geophys. Res. Lett. **24**(9), 1055–1058 (1997)

Tobie, G., Čadek, O., Sotin, C.: Solid tidal friction above a liquid water reservoir as the origin of the south pole hotspot on Enceladus. Icarus **196**(2), 642–652 (2008)

van Summeren, J., Conrad, C.P., Gaidos, E.: Mantle convection, plate tectonics, and volcanism on hot exo-earths. Astrophys. J. Lett. **736**(1), L15 (2011)

Varshalovich, D.A., Moskalev, A.N., Khersonskii, V.K.: Quantum Theory of Angular Momentum: Irreducible Tensors, Spherical Harmonics, Vector Coupling Coefficients, 3nj Symbols. World Scientific, Singapore (1988)

Wahl, S.M., Hubbard, W.B., Militzer, B.: The Concentric Maclaurin Spheroid method with tides and a rotational enhancement of Saturn's tidal response. Icarus **282**, 183–194 (2017)

Weiss, L.M., Marcy, G.W.: The mass-radius relation for 65 exoplanets smaller than 4 Earth radii. Astrophys. J. Lett. **783**(1), L6 (2014)

Zeng, L., Sasselov, D.D., Jacobsen, S.B.: Mass-radius relation for rocky planets based on PREM. Astrophys. J. **819**(2), 127 (2016)